Numerical investigation of heat and mass transfer characteristics within narrow channel in a packing humidifier

Zhiyang Hu[a], Xikun Wang[a], Xiaolong Xing[b,*], Weiliang Huang[a], Zhongyang Gao[a]

[a]*Research Center of Fluid Machinery Engineering and Technology, Jiangsu University, Zhenjiang 212013, Jiangsu, China, emails: huzhiyangoo@sina.com (Z. Hu), wangxk@ujs.edu.cn (X. Wang), hwl13978724122@163.com (W. Huang), gzy15630096995@163.com (Z. Gao)*
[b]*College of Energy and Power Engineering, Nanjing University of Aeronautics and Astronautics, Key Laboratory of Thermal Management and Energy Utilization of Aircraft, Ministry of Industry and Information Technology, Nanjing, Jiangsu 210016, China, emails: 505675275@qq.com (X. Xing)*

ABSTRACT

A numerical investigation of air/water direct contact heat and mass transfer process, by means of the volume of fluid method in a packing humidifier, with a new two-dimensional model, is used to conduct the flow characteristic of falling film. Unlike previous models for humidifiers, penetration mass transfer theory is employed to predict the field of mass fraction of water vapor accurately. Meanwhile, the influences of water temperature, inlet air velocity, as well as the water vapor concentration in the air and structure parameters, on the heat and mass transfer process have been studied. It is found that the mass fraction of water vapor increases with the increase in the inlet water temperature and inlet air humidity, but decreases with the increase in the inlet air velocity. When the inlet air velocity increases from 0.5 to 2 m s^{-1}, the mass fraction of water vapor decreases from 0.029 to 0.019 kg kg^{-1} (or -34.48%), resulting in the decrease in the average mass fraction of water vapor from 0.0375 to 0.026 kg kg^{-1} (or -30.66%). The effects of inlet water temperature, inlet air humidity, and inlet air velocity under designed parameters are quantitatively assessed, which provide useful insight into the optimization and design of humidifier.

Keywords: Heat and mass transfer; User-defined function; Penetration mass transfer theory; Volume of fluid; Humidification

1. Introduction

Packing humidifier is widely used in desalination [1,2], humid air turbine cycle [3] and other systems due to its high efficiency and low cost. Packing, as a major device, plays an important role in determining the performance of the humidifier. The heat and mass transfer process mainly occurs in the packing area, which creates a thin water film in contact with the air. Therefore, it is essential to accurately predict the two-phase air/liquid heat and mass transfer process in the humidifier.

To date, numerous studies have been carried out on the heat and mass transfer process in the packing area [4,5]. Several kinds of numerical models have been developed, such as Popper model [6], Merkel model [7], and effectiveness NTU (e-NTU) model [8]. However, all the above models are based on the assumption that the properties of the liquid and gas are constant in the cross-section [9].

Regardless of which model adopted, it is of great necessity to comprehend the impacts of different boundary conditions on the heat and mass transfer process, as demonstrated by experiments. For example, Chen et al. [10] conducted experiments on the heat and mass transfer process

* Corresponding author.

in the packing bed humidifier, and found that the effects of the wet-bulb temperature of inlet humid air, as well as temperature of inlet air and water, are significant. Ahmed et al. [11] studied the capability of a desalination system using humidification–dehumidification technology though new structured packing in the humidifier, showing that if the inlet water temperature is brought up, the inlet water flow rate will increase, thus leading to significant increase in the production of distilled water. Later, Ghalavand et al. [12] demonstrated that the mathematical model with insulation effect is more precise than the model without insulation effect, with the absolute error reduced to 2.4% with reference to the experimental data. Xu et al. [13] evaluated the mass transfer coefficient for the ceramic foam packing humidifier, and found that the local mass transfer coefficient increases with the increase in inlet water or air velocity, but decreases with the increase in inlet water temperature and inlet air enthalpy. Moreover, He et al. [14] proposed a water-heated humidification–dehumidification (HDH) system to recover waste heat, and analyzed its characteristics at different parameters for heat and mass transfer process. It was shown that the modified heat capacity ratio in humidifier is an important parameter for evaluating the capability of the HDH system. In summary, the above studies are useful references for heat and mass transfer process within packing humidifier particularly in the field of chemical application. However, experiments are always time-consuming and are unable to provide the dynamic flow and thermal fields inside of the humidifier in detail.

1.1. Computational fluid dynamic simulation

With the improvement of high-performance computing and the development of numerical techniques, computational fluid dynamics (CFD) has become increasing powerful in predicting complex heat and mass transfer process, which simplifies the complexity and number of experiments. Early studies employed CFD to simulate the pressure drop of structured packing. For instance, Scott et al. [15] used Mellapak N250Y structured packing generated by subjecting a physical packing element to CT scan. In the process, flow rates were chosen so that the velocities researched would match those commonly used in the gas phase of industrial packing columns, and the pressure drop across the packing was calculated, which was shown in good agreement with experiments. Raynal and Royon-Lebeaud [16] employed CFD model to study the pressure drop of three different types of structures. It was found that the CFD model underestimates the liquid holdup by approximate 20% compared to experiments. Later, other researchers used the volume of fluid (VOF) method to predict wetting behaviors and hydrodynamic patterns in structured packing [17,18]. Rajesh et al. [19] developed three-dimensional counter flow model based on the VOF method to simulate the post combustion carbon captured by solvent absorption in a structured packed column, in which the effect of contact angle on inter-facial area and liquid holdup was investigated. However, the solutions were limited to simulate small packing zones due to the constraints of computational resources, and industrial-scale packing was almost impossible.

The micro-scale model simplifies the structured packing into a narrow channel, which solves the problem of simulating large-scale packing adopting the details of heat and mass transfer characteristics in a channel with the available computing power. Till now, there are plenty of literatures using the micro-scale model to simulate solvent absorption [20] or dehumidification performance within absorber and direct contact dehumidification units [21]. The falling film flow on different kinds of channel structures was investigated with CFD method. Luo et al. [22] conducted a two-dimensional numerical simulation to study the dynamic heat and mass transfer process of the dehumidifier and obtained accurate water vapor concentration and temperature field. Haghshenas et al. [23] conducted CFD on the pressure drop and mass transfer efficiency of counter flow in a structured packing. Moreover, to describe the influences of liquid film flow more directly and accurately, flow characteristics have been carried out by some scholars. Tong et al. [24] studied liquid film flow over triangular corrugations both numerically and experimentally. Accordingly, resonance between the free surface and the corrugations is found when the Reynolds number (Re) of the liquid flow reaches to a certain value, which has remarkable effect on mass transfer. Haroun et al. [25] used VOF method to study the impact of the liquid flow rate and structured packing geometry on mass transfer and liquid holdup. Xu et al. [26] investigated the falling film flow on an inclined steel plate with a three-dimensional model focusing on the impacts of the gas–liquid flow rate on the wetting area and velocity profile. Based on the above literature review, it is confirmed that the CFD method is appropriate for the investigation of hydrodynamic behavior and thermodynamic process in structured packing.

1.2. Purpose of this paper

Although various simulation models have been developed, they are based on the assumption that the properties of the liquid and gas are constant in the cross-section; therefore, they cannot predict water vapor concentration and temperature distribution accurately. Furthermore, most of the previous studies focused on the effects of inlet air and water temperature on the hydrodynamic performance, but the effects of the inlet air velocity and inlet air humidity on heat and mass transfer process were rarely reported. In this paper, a micro-scale channel of a counter-flow humidification employing VOF numerical model is established, with the heat and mass transfer process taken into consideration simultaneously. Meanwhile, in order to predict the heat and mass transfer performance accurately, a user defined function (UDF) is developed based on the penetration mass transfer theory [23]. In addition, the variations of water vapor concentration in the packing area for different structures, temperatures, and inlet air velocities are investigated. Therefore, the present study can serve as a valuable reference for the design and optimization of heat and mass transfer process within narrow channel in the humidifier as shown in Fig. 1.
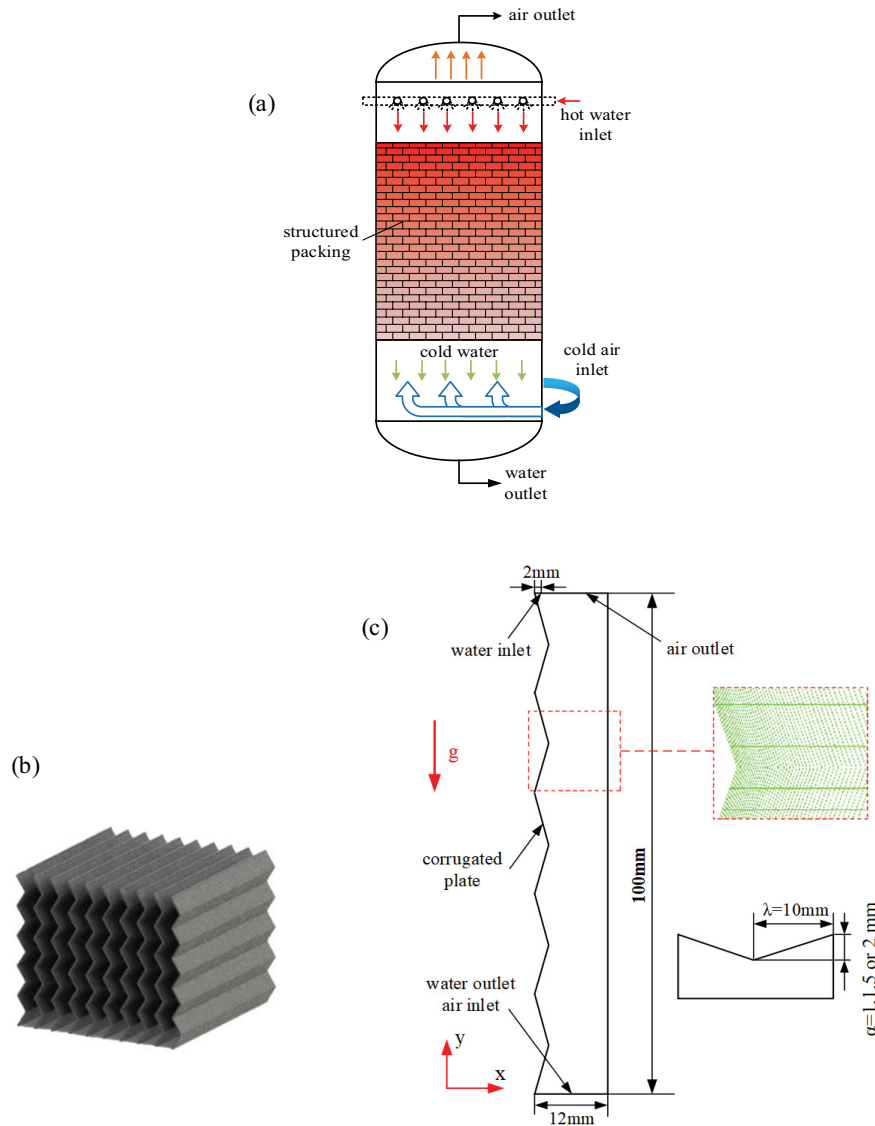
Fig. 1. (a) Schematic of the humidifier, (b) structured packing, and (c) simplified model of the corrugated channel.

2. Description of CFD model

2.1. Physical model

In this paper, the simulation is conducted for the unsteady gas–liquid flow with heat and mass transfer in a corrugated channel, Fig. 1b. The simplified model of the corrugated channel, which is designed with reference to that used in Luo et al. [22], is presented in Fig. 1c. The length of the channel is 100 mm and the width is 12 mm. The width of water inlet is 2 mm through the upper-left runner, while the width of moist air inlet is 10 mm through the bottom-right runner. In this way, the water and moist air can realize a two-phase counter-current flow.

2.2. Governing equations

The energy, momentum, mass and turbulence equations were used to describe the flow, heat and mass transfer characteristics in the structured packing zone. During

the humidification process, the hot water was cooled, and a portion of the water was converted to vapor. Concurrently, latent heat would be released as vapor phase change occurred. Consequently, the energy and mass source terms need to be added into the energy equation and species transport. The mathematical methods used in this study are described as follows.

- Mass conservation equation:

$$\frac{\partial \rho}{\partial t} + \nabla \cdot (\rho u) = S_{\mathrm{lg},k} \tag{1}$$

where $S_{\mathrm{lg},k}$ is the mass transfer source.

- Momentum conservation equation:

$$\frac{\partial}{\partial t}(\rho u) + \nabla \cdot (\rho u u) = -\nabla P + \nabla \cdot \left(\mu \left(\nabla u + \nabla u^{T}\right)\right) + \rho g + F \tag{2}$$

- Energy conservation equation:

$$\frac{\partial}{\partial t}(\rho E) + \nabla\left[V\left(\rho E + P\right)\right]\varphi_i = \nabla \cdot \left(k_{\text{eff}}\nabla T\right) + S_E \tag{3}$$

where S_E is the energy source term.

- Species transport equation:

$$\frac{\partial \alpha_q}{\partial t} + v_q \cdot \nabla \alpha_q = 0 \tag{4}$$

2.2.1. Turbulence model

Based on the work of [27,28], the Renormalisation Group (RNG) k–ε turbulence model is suitable for the simulation of narrow channel flow. The turbulence kinetic energy, k, and its rate of dissipation, ε, are obtained from the following transport equations:

$$\frac{\partial}{\partial t}(\rho k) + \frac{\partial}{\partial x_i}(\rho k u_i) = \frac{\partial}{\partial x_j}\left(\alpha_k \mu_{\text{eff}} \frac{\partial k}{\partial x_j}\right)$$
$$+ G_k + G_b - \rho\varepsilon - Y_M + S_k \tag{5}$$

$$\frac{\partial}{\partial t}(\rho\varepsilon) + \frac{\partial}{\partial x_i}(\rho\varepsilon u_i) = \frac{\partial}{\partial x_j}\left(\alpha_\varepsilon \mu_{\text{eff}} \frac{\partial \varepsilon}{\partial x_j}\right) + C_{1\varepsilon}\frac{\varepsilon}{k}\left(G_k + C_{3\varepsilon}G_b\right)$$
$$- C_{2\varepsilon}\rho\frac{\varepsilon^2}{k} - R_\varepsilon + S_\varepsilon \tag{6}$$

where α_ε is the inverse of the effective Prandtl number for ε, S_ε is the source term. The model constants $C_{1\varepsilon}$, $C_{2\varepsilon}$ and $C_{3\varepsilon}$ are 1.41, 1.66 and 0.0835, respectively.

2.2.2. VOF model

The discrimination of the gas–liquid interface adopts VOF interface tracking technology, which is widely used for the calculation free surface flow. The position of the gas–liquid interface is defined by tracking the distribution of the volume fraction of the i phase in the calculation unit φ_i. Distribution of gas–liquid interface is represented by:

$$\frac{\partial \varphi_1}{\partial t} + V \cdot \nabla \varphi_i = 0 \tag{7}$$

$$\sum_i^{j=1} \varphi_i = 1 \tag{8}$$

where φ_i is the distribution of the volume fraction of the i phase: $\varphi_i = 0$ means no phase i in the unit and $\varphi_i = 1$ means that unit is filled with phase i. Density in gas–liquid two-phase flow is presented as:

$$\rho = \varphi_l \rho_l + \varphi_g \rho_g \tag{9}$$

The solution method is similar when choosing the gas phase as the secondary phase in the VOF method.

2.3. Mass and energy source

2.3.1. Mass source

Most of the existing models are based on the film theory, which assumes that the mass transfer resistance exists in the corresponding thin layer and the mass transfer in the membrane is a diffusion process. The disadvantage of the film theory is that it can only be used to predict steady state mass transfer processes. Therefore, the penetration mass transfer theory, which ignores the mass transfer resistance at gas–liquid interface, has been proposed to study the heat and mass transfer process between water and air. Then, the total mass transfer coefficient K is calculated as follows [29]:

$$\frac{1}{K} = \frac{1}{k_l} + \frac{1}{k_g} \tag{10}$$

Here, the penetration method is employed to calculate the local mass transfer coefficients k_l and k_g:

$$k_l = 2\sqrt{\frac{D_l}{\pi\tau}} \tag{11}$$

$$k_g = 2\sqrt{\frac{D_g}{\pi\tau}} \tag{12}$$

The contact time τ is expressed as:

$$\tau = \frac{l}{u_{l,\text{surf}}} \tag{13}$$

where l is the liquid flow distance, and $u_{l,\text{surf}}$ is the surface velocity of the liquid film, which can be calculated by:

$$u_{l,\text{surf}} = 1.5Q\left(\frac{3\mu Q}{\rho g}\right)^{-1/3} \tag{14}$$

The saturated vapor pressure at the gas–liquid interface can be written as [30]:

$$P_{\text{dast}} = P_0 \times 10\exp\left(\frac{T - 273.15}{a_0 + a_1\left(T - 273.15\right) + a_2\left(T - 273.15\right)^2}\right) \tag{15}$$

where, the constants P_0, a_0, a_1 and a_2 are 610.7, 31.6639, 0.131305 and 2.63e-5, respectively.

The mass transfer source can be achieved by:

$$S_{\text{lg},k} = K\left(w_{g,e} - w_{g,b}\right)A \tag{16}$$

where $w_{g,b}$ is the humidity ratio of the moist air and $w_{g,e}$ is the humidity ratio of water vapor on liquid surface that can be calculated by:

$$w_{g,e} = 0.622 \frac{P_{dast}}{P_a - P_{dast}} \tag{17}$$

where P_a is the atmospheric pressure.

2.3.2. Energy source

In the humidification process, the heat transfer between water and air is mainly divided into two parts: the phase change heat and the sensible heat. The energy source term can be written in the following form:

$$S_E = h_k \left(T_w - T_g \right) + S_{lg,k} H_{lg,k} \tag{18}$$

where h_k is heat transfer coefficient of gas–liquid and $H_{lg,k}$ is latent heat.

3. Simulation method

The computational flow domain was meshed by structured grids using ICEM (the Integrated Computer Engineering and Manufacturing code). To accurately and efficiently calculate heat and mass transfer process, the gradient form based on structured cells was used. A more refined mesh was set near the wall of corrugated plate to capture the flow behavior. In this region, a minimum grid size of 0.006 mm was specified. As the gravitational force cannot be neglected, the body force weighted pressure discretization scheme was adopted. The pressure-based non-steady-state format was used for calculation with a very small time step ($\Delta t = 10^{-5}$-10^{-4} s). The PRESTO! Pressure interpolation scheme was utilized, which is very suitable for pressure–velocity coupling [31]. The convection term adopted the first-order upwind differencing to accelerate the calculation. As for tracking of the gas–liquid interface, the geo-reconstruct format was selected for its higher accuracy. The mass and energy source items were written and accessed through user defined functions (UDF) macro commands provided by Fluent. The average mass fraction of water vapor in the moist air at gas outlet boundary was monitored to determine whether the stable state was achieved. As presented in Fig. 2, if the above parameters start to oscillate around a certain value, it is regarded as pseudo-steady-state and the calculation is completed.

Initially, the whole computational domain was occupied by moist air, that is, the volume fraction of air was 1 and the volume fraction of liquid was 0 at the beginning of calculation. The water inlet and air outlet are set as velocity inlet boundary. Since there is no clear line between water outlet and air inlet, the whole bottom is set as pressure outlet boundary. The corrugated plate and the wall are set as no-slip boundary condition. The inlet velocity and temperature of water and inlet humidity and temperature of the moist air could be set and modified at the boundary conditions. For the moist air, the database of Fluent has all its physical properties. The user only needs to set the two components of air and water vapor, and mix them with the relevant formulas contained in the software.

If the gas–liquid flow and heat and mass transfer conditions are calculated simultaneously, the calculation will be slow to reach convergence. Thus, a two-step calculation strategy is adopted. Firstly, the pure gas–liquid flow is calculated. When the gas–liquid flow is stable, the UDF is used to import the mass and energy source terms for calculation

4. Validity of the model

4.1. Verification of grid independence

To ensure the accuracy of simulation results, five types of grids of different sizes are used for the grid independence
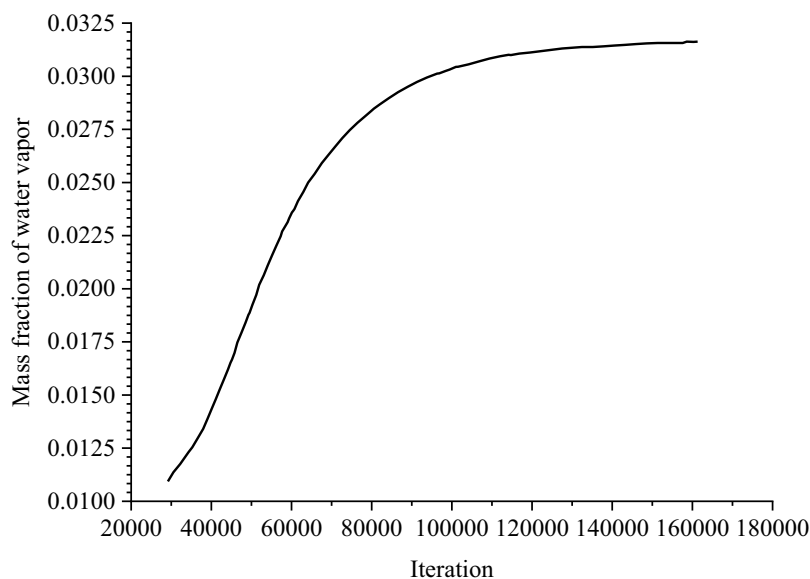

Fig. 2. Convergence history of mass fraction of water vapor in outlet air.

test. In order to save computing resources, the grid density decreases gradually from the water to the air phase. Near the wall of water flow, the first layer of grids is kept at y^+~1 corresponding to a grid size of 0.01 mm. The temperature of air and the mass fractions of water vapor at the gas outlet are monitored under the same boundary conditions to verify the simulation results.

The calculated air conditions at the gas outlet with the five types of grids are showed in Fig. 3, confirming that grid size does have an impact on the simulation results. The difference in the outlet air temperature predicted by the third grid (68 × 330) and fourth grid (80 × 330) is within 0.15 K. As for the mass fraction of water vapor at gas outlet, the difference between the third and fourth grids is also negligibly small. Considering the computing resources and cost, the grid size 68 × 330 is selected for all the simulations.

4.2. Verification of heat and mass transfer performances

To further justify the established model, the calculation results are compared with those published in literature [32], as shown in Fig. 4. The data agreement is excellent, with the error controlled within 7%, which proves that the mathematical model and UDF adopted in this paper are completely reasonable.

4.3. Film thickness verification

The state of water is mainly film flow, so the thickness of the liquid film is an important indicator of the flow state. The mean film thickness δ for laminar flow can be achieved by the Nusselt film empirical formula, which can be expressed as:

$$\delta = \left(\frac{3\mu \mathrm{Re}}{g} \right)^{1/3} \tag{19}$$

To verify the accuracy of the model in the flow state, the average thickness of water film calculated by simulation model is compared with that predicted by empirical formula, as shown in Fig. 5. Again, the simulation results agree well with the empirical results, with the maximum error of ±16%. Therefore, it is reliable to apply the present model to simulate the flow state of humidification.

5. Results and discussion

Based on the established model, the heat and mass transfer process has been investigated under various conditions. Table 1 summarizes the different calculating conditions used in the present study.

5.1. Influences of structural parameters

Structural parameters of the model are provided in Table 2. The parameter ratio (α/λ) is varied from 0 to 0.2. It is observed that when $\alpha/\lambda > 0.2$ water film splashes, accumulates in the trough and cannot be effectively updated, which is not conductive to heat and mass transfer process. Therefore, the parameter ratio in this paper is controlled within 0.2, which can stabilize the distribution of the water film.

Fig. 6 shows that different corrugated structures have different mass fractions of water vapor at air outlet. Initially, the mass fraction of water vapor at air outlet increases with the increase of α/λ. However, it begins to decrease when α/λ is greater than 0.15. That is to say, the mass fraction of water vapor at outlet air attains the maximum at $\alpha/\lambda = 0.15$. The reason is that when α/λ increases to 0.15, local flow separation and water retention occurs, resulting in slowing down of heat and mass transfer process.

The contours of mass fraction of water vapor and temperature under different parameter ratios are demonstrated
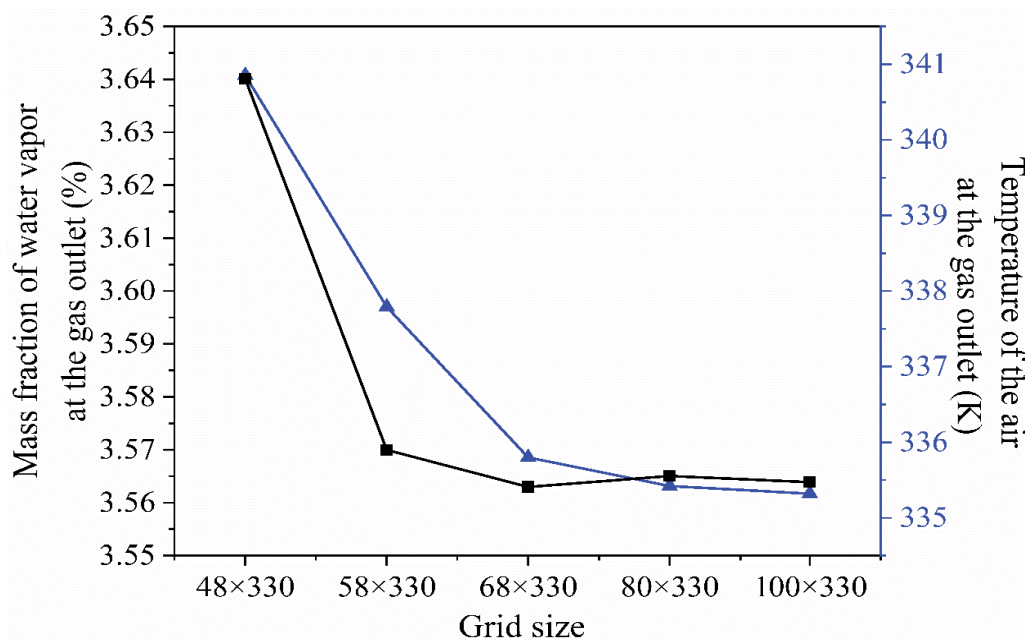

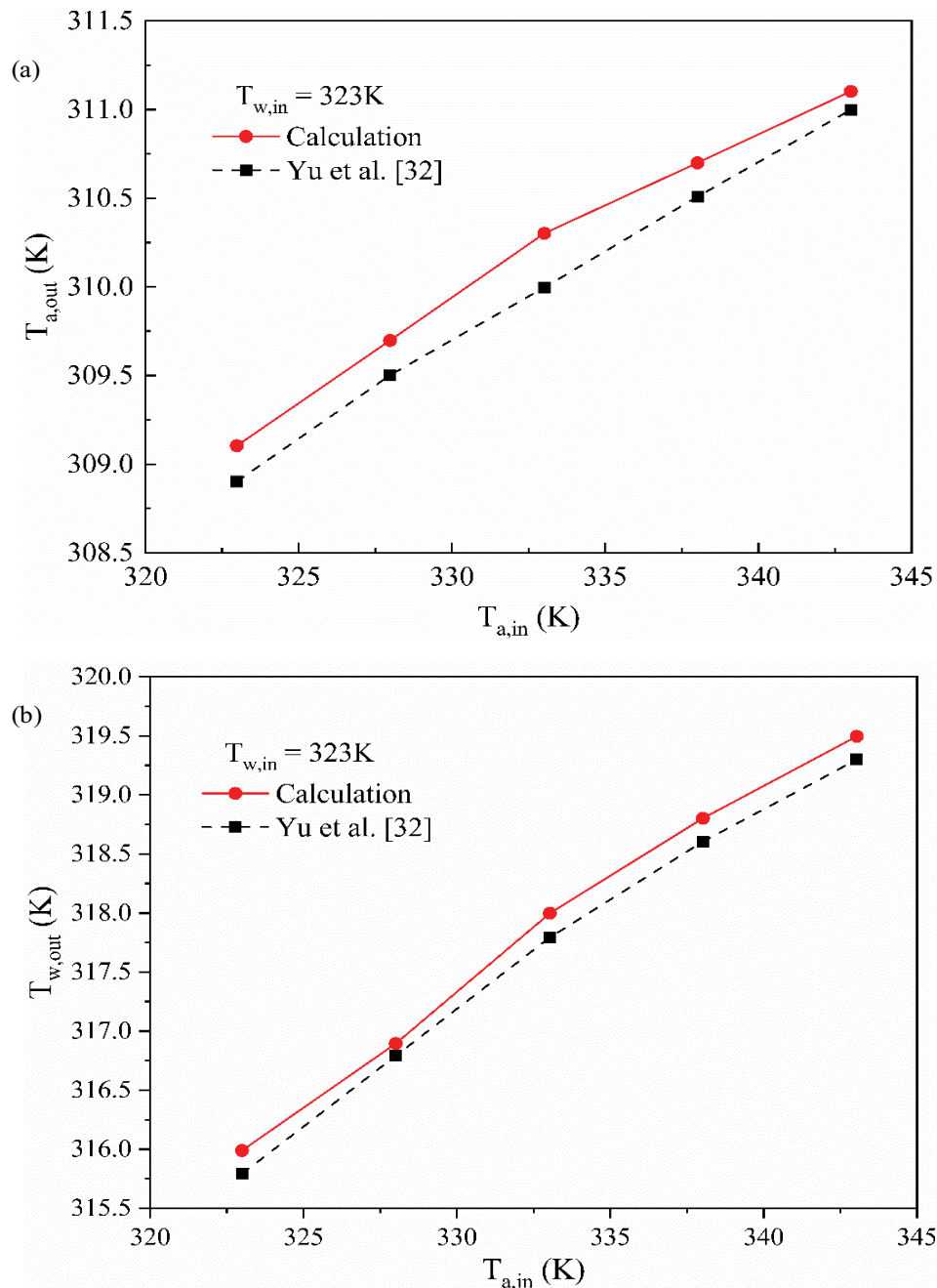Fig. 3. Air conditions at the gas outlet with five types of grids.

Fig. 4. Comparison of the experimental [32] and numerical results: (a) water outlet temperature and (b) air outlet temperature.

in Figs. 7 and 8, respectively. It is observed that the humidification performance of corrugated channel is better than that of flat channel. There are two factors affecting the heat and mass transfer performance of the corrugated channel. On the one hand, the corrugated channel increases the gas–liquid contact area as compared to the flat channel, thereby enhancing the mass transfer process. On the other hand, the gas–liquid contact time is longer, which is also favorable for the mass transfer process. Combination of the above two factors results in the mass fraction of water vapor at air outlet to be more uniformly distributed with higher magnitude.

Fig. 9 shows the liquid film distribution for different values of α/λ. Contours of liquid volume fraction are shown in Fig. 9a. At $\alpha/\lambda = 0$ (i.e., un-corrugated case), the liquid film flows vertically downward along the flat plate to form a complete liquid film. With α/λ Increasing, the gas–liquid contact area increases, and the liquid film confirms with the corrugated wall, exhibiting a wavy shape. This situation is conducive to heat and mass transfer, so as to improve the humidification efficiency of the humidifier. However, α/λ cannot be too large. For $\alpha/\lambda = 0.3$, for example, the liquid film breaks in the middle of the corrugated plate. Fig. 9b shows the distribution of liquid film thickness
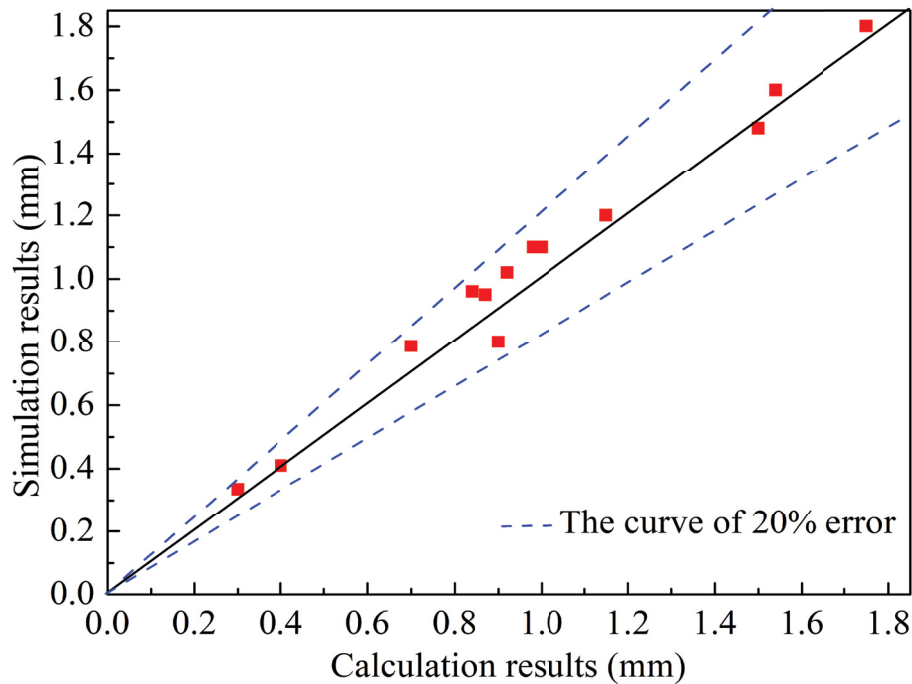
Fig. 5. Comparison of water thickness between simulation results and Nusselt empirical prediction.

Table 1
Summary of calculating conditions

	Water			Air	
Parameter	$T_{w,in}$ (K)	$u_{w,in}$ (m s^{-1})	$T_{a,in}$ (K)	$w_{a,in}$ (kg kg^{-1})	$u_{a,in}$ (m s^{-1})
Basic point	350	1.0	300	1.1	1.0
Range	310–350	1.0	300	1.1–3.2	0.5–2.0

Table 2
Structure parameters of physical model

Structure	α (mm)	λ (mm)	α/λ
Flat plate	0	10	0
Corrugated plate 1	1.0	10	0.10
Corrugated plate 2	1.5	10	0.15
Corrugated plate 3	2.0	10	0.20

for five different parameter ratios (α/λ). At α/λ = 0, the thickness of liquid film decreases monotonically to only about 1 mm at the outlet. At α/λ > 0, the distribution is in wave form, and becomes increasingly sharp with the increase in α/λ. Finally, at α/λ = 0.3, the thickness of liquid film at troughs is much greater; the accumulation of liquid causes the fracture of liquid film, which is unfavorable to the heat and mass transfer.

5.2. Influences of inlet air velocity

As highlighted in the literature review, the impact of the inlet air velocity on humidification process has been rarely investigated previously. However, the inlet air velocity would significantly affect the state of water film and the gas–liquid contact time, and hence the heat and mass transfer process. Thus, the inlet air velocity is varied and the results under different inlet air velocities are presented in Figs. 10 and 11.

The influences of inlet air velocity on the mass fraction of water vapor at x = 8 mm are illustrated in Fig. 10a and the surface contact angle is 20°. When the inlet air velocity increases from 0.5 to 2 m s^{-1}, the corresponding

mass fraction of water vapor decreases from 0.029 to 0.019 kg kg^{-1}, and the rate of change is -34.48%. The reason is that the air–liquid contact time becomes shorter at higher inlet air velocity, which is unfavorable for the mass transfer process. At the same time, it is observed that the mass fraction of water vapor decreases at y = 90 mm. The reason is that the driving force for mass transfer at the outlet is weakened after moist air is humidified through the inlet. The average mass fraction of water vapor is shown in Fig. 10b. When the air velocity increases from 0.5 to 2 m s^{-1}, the average mass fraction of water vapor decreases from 0.0375 to 0.026 kg kg^{-1}, and the rate of change is -30.66%. Moreover, it is discovered that the average mass fraction of water vapor fluctuates in a wave shape along y direction. This implies water accumulation in the trough, which is conductive to heat and mass transfer process, as demonstrated by a downward trend in the mass fraction of water vapor. Otherwise, the water vapor mass fraction displays an upward trend at the peak due to the increase in turbulence caused by fluctuation of water film.

The contours of mass fraction of water vapor in the interior of the humidifier are demonstrated in Fig. 11. The heat and mass transfer process starts from the gas–liquid
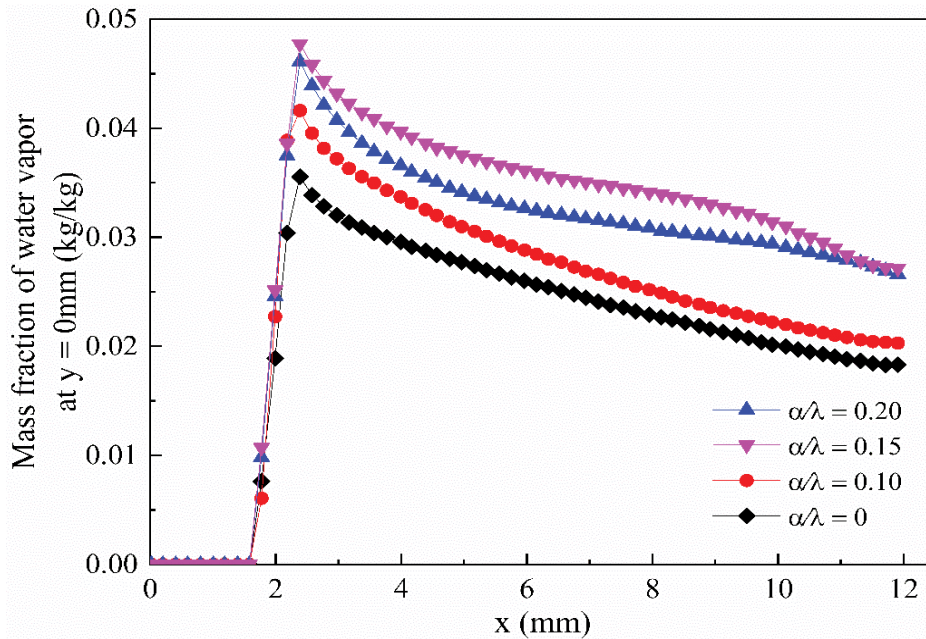
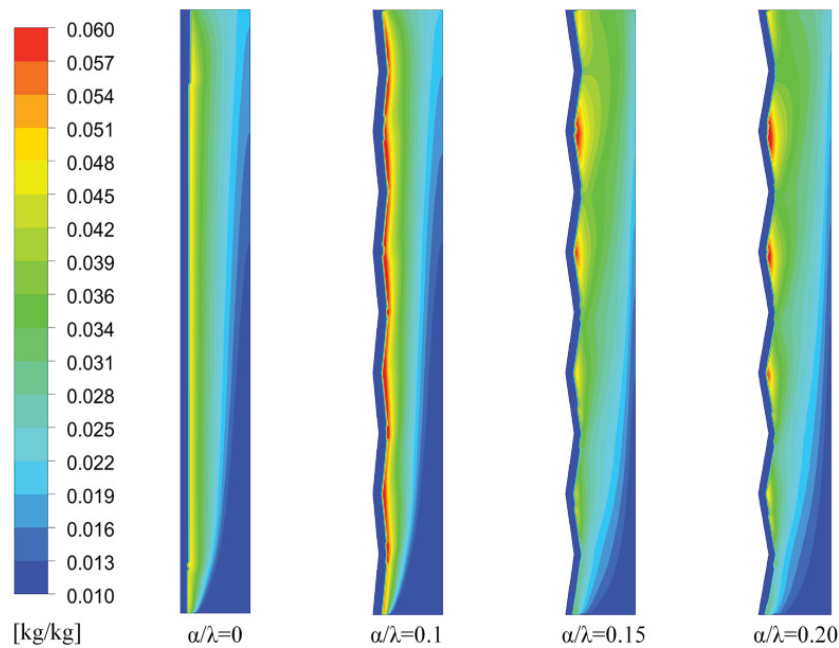Fig. 6. Mass fraction of water vapor for different structures.

Fig. 7. Contour of mass fraction of water vapor for different structures.

interface and then extends to the gas phase, wherein moist air is continuously humidified. In order to optimize the humidification system, the air velocity should be set appropriately by taking the packing size into account, including the packing length and width. A lower air velocity will certainly provide longer contact time and larger contact area for mass transfer. However, the air velocity cannot be too low due to technical requirements and stable operation of equipment. Note that for the case of inlet air velocity

above 1.0 m s⁻¹, the width of the channel should be reduced, as there is a large zone in blue color (i.e., without mass transfer) in the contour plot.

Moreover, the gradient of mass fraction of water vapor in the whole channel is analyzed and presented in Fig. 12. The y-values for the cross sections vary from 20 to 80 mm. It can be seen that at y = 20 mm, the slope (or gradient) of mass fraction of water vapor becomes nearly horizontal near the wall surface, which is different from that at two
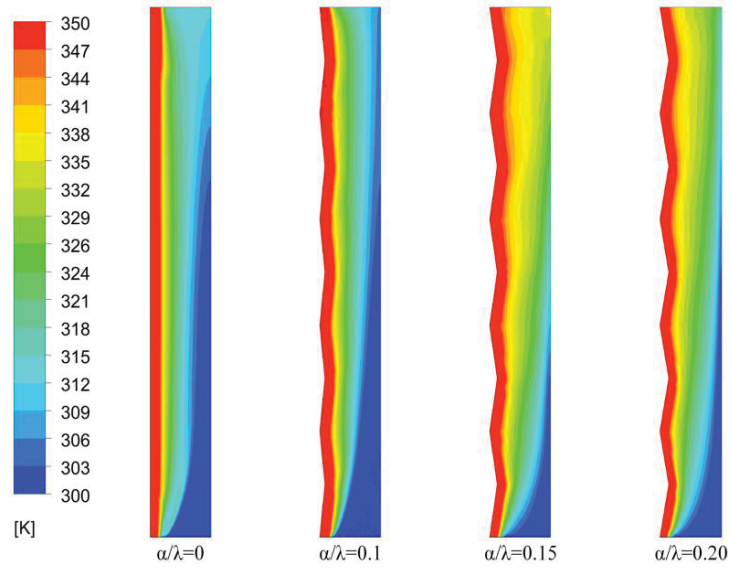
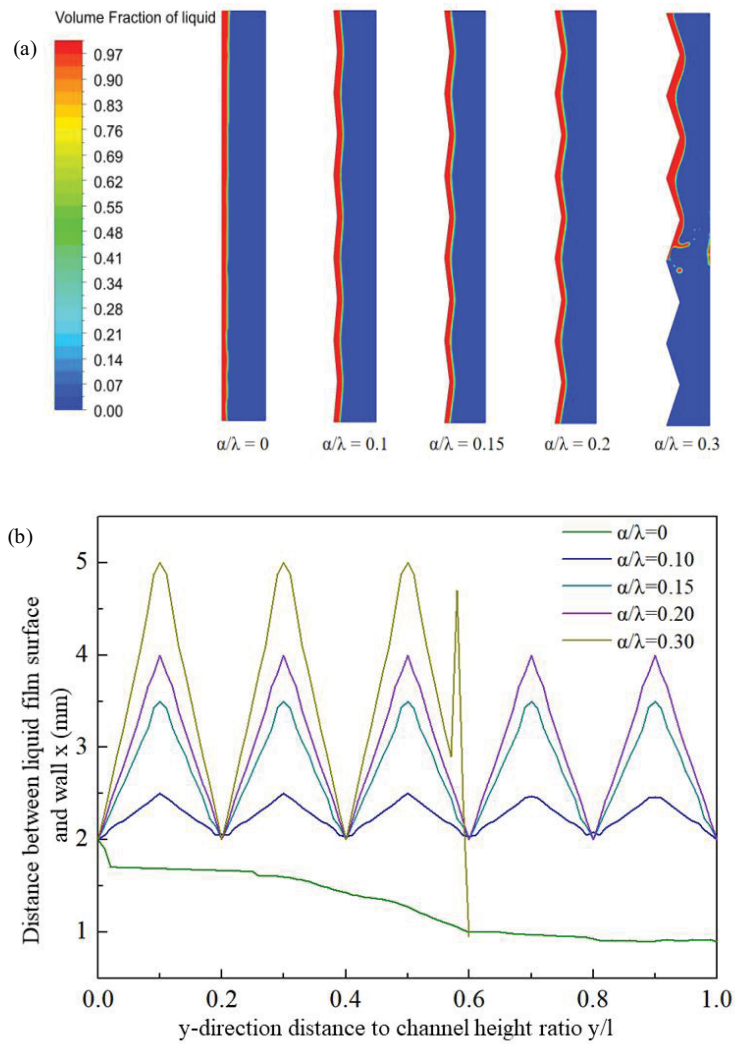Fig. 8. Contour of temperature for different structures.

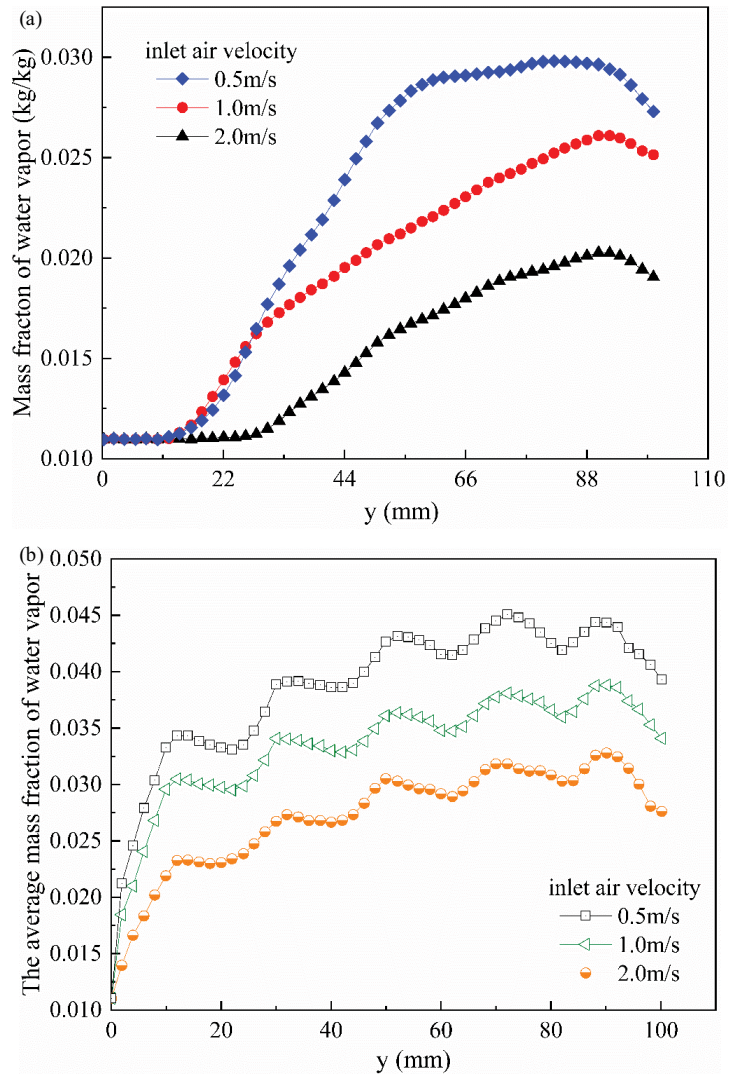Fig. 9. Liquid film thickness distribution for different structures.

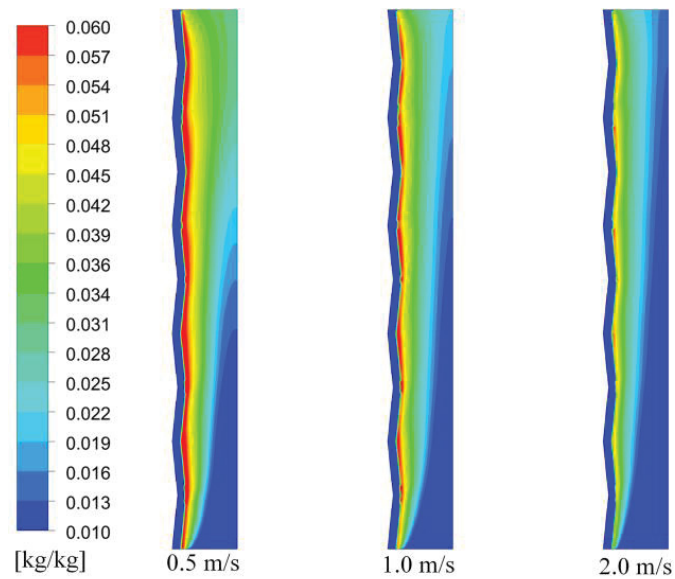Fig. 10. Mass fraction of water vapor under different inlet air velocities.

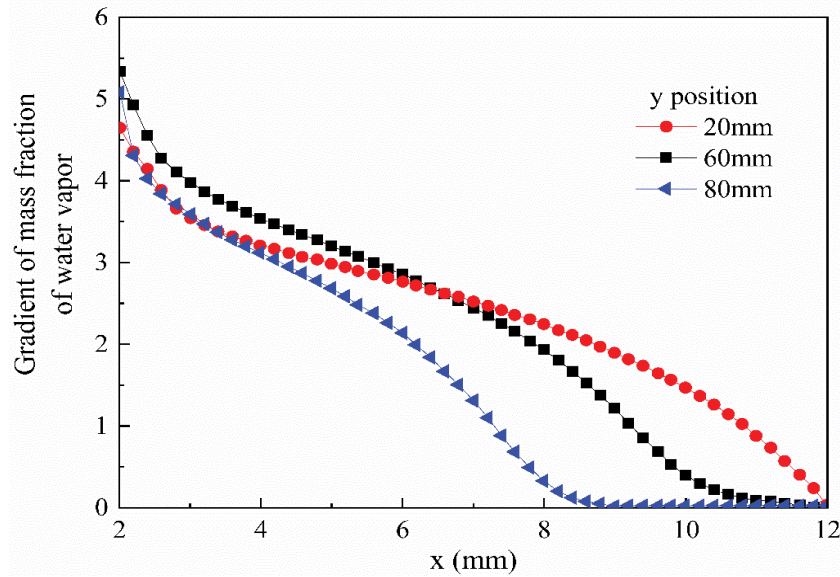Fig. 11. Contour of mass fraction of water vapor under different inlet air velocities at $\alpha/\lambda = 0.15$.

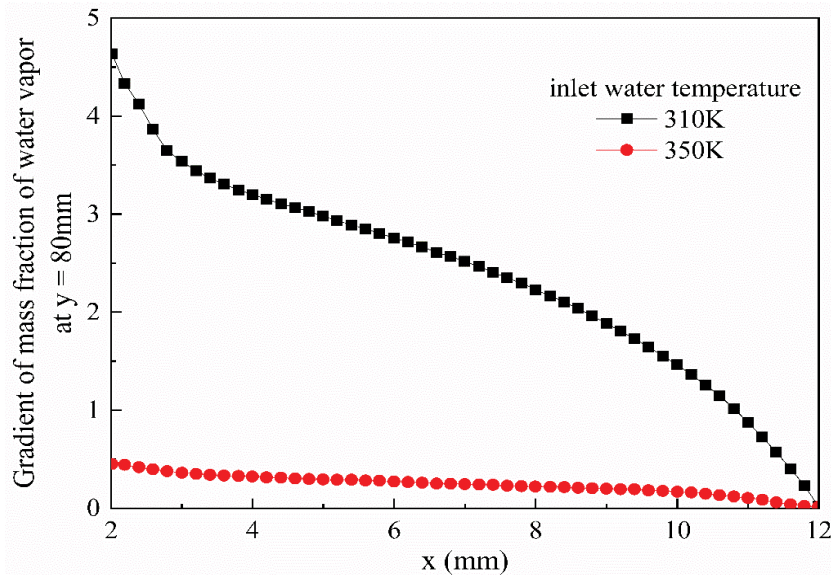Fig. 12. Gradient of mass fraction of water vapor at different *y* values.

Fig. 13. Mass fraction of water vapor under different inlet water temperature.

other locations. As shown in Eqs. (11) and (12), the slope of the curve represents the mass transfer rate. For the curve at *y* = 20 mm, the mass transfer rate decreases at *x* = 2-8 mm, but at *x* = 8-12 mm it is rising. This is because that near the outlet, the humidity of air increases as compared to that at the inlet. Due to the narrower channel width, the thickening of the viscous boundary layer near the wall at *x* = 8-12 mm will cause a longer dwelling time of air over there. This leads to an increase in the mass transfer rate between water and air.

5.3. *Influences of inlet water temperature*

For gas–liquid falling film flow, there are driving forces due to the temperature difference in sensible heat transfer and the moisture content difference in latent heat transfer, both of which give rise to heat and mass transfer between gas and liquid along the wall. On the one hand, increasing the temperature difference between them can improve the sensible heat driving force. On the other hand, the increase in temperature can enhance the evaporation of water and affect the mass transfer process between gas and liquid.

Fig. 13 illustrates the humidification performance in terms of mass fraction of water vapor in moist air at different water temperatures. Obviously, the mass fraction of water vapor displays a distinct increase with the increment of water temperature. Specifically, the mass fraction of water vapor increases from 0.016 to 0.036 kg kg^{-1} when water temperature increases from 310 to 350 K, which
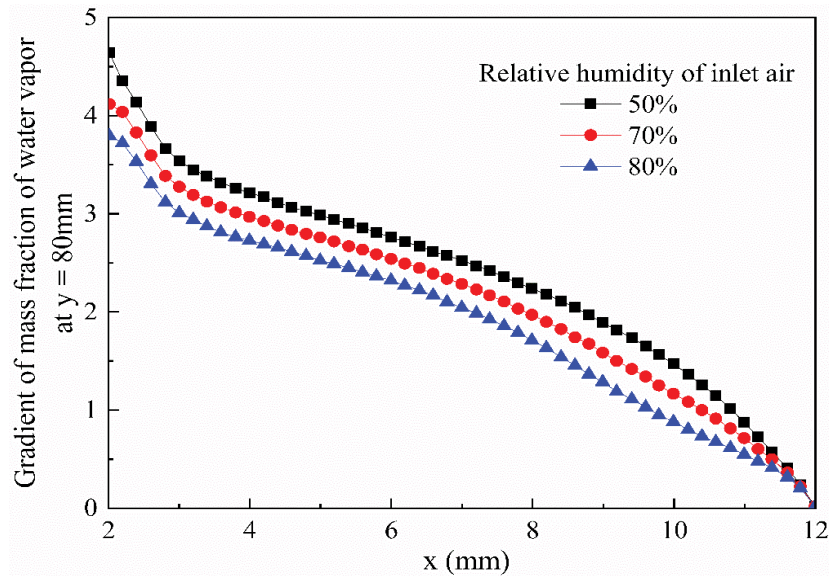
Fig. 14. Mass fraction of water vapor under different inlet air humidity.

leads to the increment of water vapor pressure and mass transfer driving force.

5.4. Influences of relative humidity of inlet air

With other inlet parameters fixed, the increase of mass fraction of water vapor at air inlet will weaken the driving force of mass transfer between the air and water. Fig. 14 presents the gradient of mass fraction of water vapor at the same cross section ($y = 80$ mm) under different water vapor concentrations of inlet air. It is found that the gradient of mass fraction of water vapor becomes more and more vague with the increase of the water vapor concentration at air inlet.

In the case of constant water inlet conditions, the larger the mass fraction of inlet water vapor, the smaller mass transfer driving force, attenuating the humidification effect. At locations far from the water film, the mass transfer gradient can be nearly zero, indicating that no mass transfer occurs there.

6. Conclusions

Humidification in humidifier poses a complex multiphase problem, which involves many factors including the structural parameters of the corrugated channel and the boundary conditions. To gain a better understanding of the micro-scale heat and mass transfer phenomena in the humidifier, a two-dimensional corrugated channel model was proposed and developed. The following conclusions are obtained:

- The two-dimensional multiphase-VOF model developed can accurately predict the two-phase gas–liquid heat and mass transfer process within structured packing humidifier. The numerical simulation results agree well with the reference results within a discrepancy of less than 6%.

- The corrugated channel has an optimal parameter ratio of $\alpha/\lambda = 0.15$ to achieve the best heat and mass transfer performance.
- Raising the inlet air velocity will reduce the average mass fraction of water vapor. When inlet air velocity increases from 0.5 to 2 m s^{-1}, the mass fraction of water vapor at air outlet decreases from 0.029 to 0.019 kg kg^{-1} (or -34.48%), resulting in the decrease in the average mass fraction of water vapor from 0.0375 to 0.026 kg kg^{-1} (or -30.66%).
- The simulation results show that the penetration mass transfer theory can faithfully predict the water vapor concentration field, local gradients of water vapor concentration and influence of mass transfer on the film surface waves of the humidifier at the location $x = 8$ mm.
- The heat and mass transfer performance of the humidifier is subject to the influences of boundary conditions, that is, inlet air velocity, inlet water temperature and inlet air humidity, which determine the mass transfer driving force. Lower inlet air velocity leads to a longer gas–liquid contact time and hence better humidification performance.

It is noteworthy that the present study focuses on the gas–liquid mass and heat transfer characteristics in a simplified two-dimensional corrugated channel model. Further research is required to optimize the structural and flow parameters, as well as to evaluate the performance of the actual packing humidifier, such as humidification efficiency, pressure drop, economic viability, etc.

Symbols

A	—	Mass transfer area, m^2
D_g	–	Diffusion coefficient of moist air, m^2 s^{-1}
D_l	–	Diffusion coefficient of liquid, m^2 s^{-1}
F	—	Momentum source term, N m^{-3}
g	—	Acceleration of gravity, kg m^{-1} s^{-3}

h_k	—	Heat transfer coefficient of gas–liquid, W m^{-2} K^{-1}
$H_{\text{lg},k}$	—	Latent heat of evaporation, J kg^{-1}
i	—	Number of the phases
k	—	Turbulence kinetic energy, m^2 s^{-2}
K	—	Overall mass transfer coefficient, kg m^{-2} s^{-1}
k_g	—	Local mass transfer coefficient of gas phase, kg m^{-2} s^{-1}
k_l	—	Local mass transfer coefficient of liquid phase, kg m^{-2} s^{-1}
l	—	Flow distance, m
P_a	—	Atmospheric pressure, Pa
P_{dast}	—	Saturated vapor pressure at the gas–liquid interface, Pa
P_0	—	Constant pressure, Pa
Q	—	Mass flow rate of liquid, kg s^{-1}
Re	—	Reynolds number
S	—	Mass of the product water, kg
S_E	—	Energy source term, W m^{-3}
$S_{\text{lg},k}$	—	Mass transfer source at the phase interface, kg m^{-3}
S_ε	—	User-defined source terms, kg m^{-1} s^{-3}
T	—	Temperature, K
u	—	Velocity vector, m s^{-1}
$u_{l,\text{surf}}$	—	Liquid surface velocity, m s^{-1}
$u_{a,\text{in}}$	—	Inlet air velocity, m s^{-1}
$u_{w,\text{in}}$	—	Inlet water velocity, m s^{-1}
$w_{g,b}$	—	Humidity ratio of the moist air, kg kg^{-1}
$w_{g,e}$	—	Humidity ratio of water vapor on liquid surface, kg kg^{-1}
ww	—	Liquid to gas ratio
$x_{a,\text{in}}$	—	Mass fraction of water vapor at the gas inlet, kg kg^{-1}
Y_M	—	Overall dissipation rate, kg m^{-1} s^{-3}

Greek

α	—	Amplitude, mm
μ	—	Dynamic viscosity, kg m^{-1} s^{-1}
ρ	—	Density, kg m^{-3}
ε	—	Dissipation rate of turbulence kinetic energy, m^2 s^{-3}
τ	—	Contact time, s
θ	—	Contact angle, °
ψ	—	Volume fraction
λ	—	Wavelength, mm
π	—	PI
δ	—	Film thickness, mm

Subscripts

a	—	Air
eff	—	Effective
g	—	Gas phase
i	—	The i-th species
in	—	Inlet
l	—	Liquid phase
out	—	Outlet
w	—	Water

References

[1] W.F. He, H.X. Yang, T. Wen, D. Han, Thermodynamic and economic investigation of a humidification dehumidification desalination system driven by low grade waste heat, Energy Convers. Manage., 183 (2019) 848–858.

[2] D. Han, W.F. He, C. Ji, L. Huang, Thermodynamic analysis of a novel evaporation and crystallization system based on humidification processes at ambient temperature, Desalination, 439 (2018) 108–118.

[3] Y. Hui, Y.Z. Wang, S.L. Weng, Experimental investigation of pressurized packing saturator for humid air turbine cycle, Appl. Therm. Eng., 62 (2014) 513–519.

[4] W.F. He, L. Huang, J.R. Xia, W.P. Zhu, D. Han, Y.K Wu, Parametric analysis of a humidification dehumidification desalination system using a direct-contact dehumidifier, Int. J. Therm. Sci., 120 (2017) 31–40.

[5] W.F. He, D. Han, T. Wen, H.X. Yang, J.J. Chen, Thermodynamic and economic analysis of a combined plant for power and water production, J. Cleaner Prod., 228 (2019) 521–532.

[6] J.J. Chen, D. Han, W.F. He, Characteristic analysis of heat and mass transfer process within structured packing humidifier, J. Braz. Soc. Mech. Sci. Eng., 361 (2019) 1–15.

[7] Z. Xu, Y.C. Xie, Y.H. Xiao, A compact packing humidifier for the micro humid air turbine cycle: Design method and experimental evaluation, Appl. Therm. Eng., 125 (2017) 727–734.

[8] H. Jaber, R.L. Webb, Design of cooling towers by the effectiveness-NTU method, J. Heat Transfer, 111 (1989) 837–843.

[9] T.F. Ke, X. Huang, X. Ling, Numerical and experimental analysis on air/water direct contact heat and mass transfer in the humidifier, Appl. Therm. Eng., 156 (2019) 310–323.

[10] J.J. Chen, D. Han, W.F. He, Y. Liu, J.M. Gu, Theoretical and experimental analysis of the thermodynamic and economic performance for a packed bed humidifier, Energy Convers. Manage., 206 (2020) 112479, doi: 10.1016/j.enconman.2020.112497.

[11] H.A. Ahmed, I.M. Ismail, W.F. Saleh, Experimental investigation of humidification–dehumidification desalination system with corrugated packing in the humidifier, Desalination, 410 (2017) 19–29.

[12] Y. Ghalavand, A. Rahimi, M.S. Hatamipour, Mathematical modeling for humidifier performance in a compression desalination system: insulation effects, Desalination, 433 (2018) 48–55.

[13] Z. Xu, Y. Xie, F. Zhang, Development of mass transfer coefficient correlation for a ceramic foam packing humidifier at elevated pressure, Appl. Therm. Eng., 133 (2018) 560–565.

[14] W.F. He, D. Han, W.P. Zhu, C. Ji, Thermo-economic analysis of a water-heated humidification-dehumidification desalination system with waste heat recovery, Energy Convers. Manage., 160 (2018) 182–190.

[15] A. Scott, R. Michael, Perkins, R. Bruce, Computational fluid dynamics simulation of structured packing, Ind. Eng. Chem. Res., 52 (2013) 2032–2045.

[16] L. Raynal, A. Royon-Lebeaud, A multi-scale approach for CFD calculations of gas–liquid flow within large size column equipped with structured packing, Chem. Eng. Sci., 62 (2007) 7196–7204.

[17] C.W. Hirt, B.D. Nichols. Volume of fluid (VOF) method for the dynamics of free boundaries, J. Comput. Phys., 39 (1981) 201–225.

[18] C.R. Kharangate, I. Mudawar, Review of computational studies on boiling and condensation, Int. J. Heat Mass Transfer, 108 (2017) 1164–1196.

[19] K. Rajesh, E. Janine, X. Sun, Multiphase flow studies for microscale hydrodynamics in the structured packed column, Chem. Eng. J., 353 (2018) 949–963.

[20] P. Chasanis, A. Lautenschleger, E. Kenig, Numerical investigation of carbon dioxide absorption in a falling-film micro-contactor, Chem. Eng. Sci., 65 (2010) 1125–1133.

[21] T. Wen, Y.M. Luo, L. Lu, A novel 3D simulation model for investigating liquid desiccant dehumidification performance based on CFD technology, Appl. Energy, 240 (2019) 486–498.

[22] Y.M. Luo, H.X. Yang, L. Lu, Liquid desiccant dehumidifier: development of a new performance predication model based on CFD, Int. J. Heat Mass Transfer, 69 (2014) 408–416.

[23] F.M. Haghshenas, M. Zivdar, R. Rahimi, E.M. Nasr, A. Afacan, K. Nandakumar, K. Chuang, CFD simulation of mass transfer efficiency and pressure drop in a structured packed distillation column, Chem. Eng. Technol., 30 (2007) 854–861.

[24] Z.Y. Tong, A. Marek, W.R. Hong, J. Repke, Experimental and numerical investigation on gravity-driven film flow over triangular corrugations, Ind. Eng. Chem. Res., 52 (2013) 15946–15958.

[25] Y. Haroun, L. Raynal, D. Legender, Mass transfer and liquid hold-up determination in structured packing by CFD, Chem. Eng. Sci., 75 (2012) 342–348.

[26] Y. Xu, J. Yuan, J. Repke, G. Wozny, CFD study on liquid flow behavior on inclined flat plate focusing on effect of flow rate, Eng. Appl. Comput. Fluid Mech., 6 (2012) 186–194.

[27] F. Gu, C.J. Liu, X.G. Yuan, G.C. Yu, CFD simulation of liquid film flow on inclined plates, Chem. Eng. Technol., 27 (2004) 1099–1104.

[28] A. Ataki, H.-J. Bart, Experimental and CFD simulation study for the wetting of a structured packing element with liquids, Chem. Eng. Technol., 29 (2006) 336–347.

[29] R.B. Bird, W.E. Stewart, Lightfoot E N, Transport Phenomena, Wiley, New York, 1960.

[30] G.B. Liu, Y. Hui, Y.Z. Wang, Numerical simulation of the mass transfer in gas–liquid falling film flow on the vertical plate, Gas Turbine Technol., 25 (2012) 34–39.

[31] L. Zhang, E. Hihara, F. Massuoka, C.B. Dang, Experimental analysis of mass transfer in adiabatic structured packing dehumidifier/regenerator with liquid desiccant, Int. J. Heat Mass Transfer, 53 (2010) 2856–2863.

[32] J. Yu, S.M. Jin, Y.J. Xia, Experimental and CFD investigation of the counter-flow spray concentration tower in solar energy air evaporating separation saline wastewater treatment system, Int. J. Heat Mass Transfer, 144 (2019) 118621, doi: 10.1016/j.ijheatmasstransfer.2019.118621.